Physics of Fluids

Pair trajectories of uncharged conducting spheres in an electric field

Cite as: Phys. Fluids **35**, 033311 (2023); https://doi.org/10.1063/5.0142014
Submitted: 10 January 2023 • Accepted: 22 February 2023 • Accepted Manuscript Online: 23 February 2023 • Published Online: 13 March 2023

Natarajan Thiruvenkadam, Pijush Patra, Vishwanath Kadaba Puttanna, et al.

Physics of Fluids ARTICLE scitation.org/journal/phf

Pair trajectories of uncharged conducting spheres in an electric field

Cite as: Phys. Fluids **35**, 033311 (2023); doi: 10.1063/5.0142014
Submitted: 10 January 2023 · Accepted: 22 February 2023 ·
Published Online: 13 March 2023

Natarajan Thiruvenkadam,[1] Pijush Patra,[2] Vishwanath Kadaba Puttanna,[1] and Anubhab Roy[2,a)]

AFFILIATIONS

[1]Department of Mathematical and Computational Sciences, National Institute of Technology Karnataka, Surathkal 575025, India
[2]Department of Applied Mechanics, Indian Institute of Technology Madras, Chennai 600036, India

[a)]Author to whom correspondence should be addressed: anubhab@iitm.ac.in

ABSTRACT

In this paper, we study the role of electrostatic forces on pair trajectories of two uncharged conducting spheres subject to an external electric field. We consider the hydrodynamic interactions between the spheres as they move relative to one another. Previous studies have shown that electric-field-induced forces on a two-sphere system are always attractive, except for the configuration when the line joining the centers is perpendicular to the external electric field. In the current study, we derive the asymptotic form of the interparticle force induced by the electric field in the lubrication limit for arbitrary size ratios. The attractive electric force diverges as the separation approaches zero. Thus, our calculation shows that the electric-field-induced forces can overcome the continuum lubrication resistance and allow finite time contact between the surfaces of two spherical conductors. We calculate the asymptotic variation of interparticle separation using the near-field asymptotic expressions for the electric-field-induced forces, exploring the role of hydrodynamic interactions in interparticle motion parallel and perpendicular to the electric field.

I. INTRODUCTION

The behavior of conducting particles in an external electric field is crucial to many industrial applications such as phase separations,[1] electrowetting,[2] emulsification,[3] and lab-on-a-chip manipulations. In oil industries, the electrocoalescence of a water-in-oil emulsion is crucial to the efficient and quick dehydration of crude oil.[4–6] The electric-field-enhanced coagulation (of rigid particles) or coalescence (of liquid droplets) also has applications in atmospheric processes. The rapid coalescence due to high electric field strength is a dominant growth mechanism for droplets in strongly electrified clouds, particularly before lightning.[7] The electric field intensity inside natural clouds is $O(10^3\ \mathrm{Vm}^{-1})$, whereas the same inside thunderclouds is $O(10^5\ \mathrm{Vm}^{-1})$ (see Ref. 7 who presented a summary of several field observations on electric field strength in different types of clouds). The electric field applied to a suspension of uncharged spherical conducting particles helps to flocculate the suspension. Thus, particle–particle interactions in an external electric field are a growing field of interest. In this study, we restrict our focus to dilute suspensions, where only pairwise interactions are significant. Here, we explore the near-field dynamics of two uncharged conducting spheres interacting hydrodynamically in an imposed electric field.

An external electric field acting on a drop suspended in a fluid medium of different permittivities and conductivities creates electrical stresses, which shear the fluid interfaces into motion[8] (i.e., results in electrohydrodynamic flows). The complicated interaction between the electric-field-induced and viscous fluid stresses causes either oblate or prolate drop deformation in a weak field. To predict the drop shape of a weakly conducting drop, Taylor[9] developed the leaky dielectric model (LDM) in the small deformation limit. When the applied electric field is strong, the drop exhibits different complex dynamics such as breakup[10,11] streaming either from the drop poles[12–14] or equator[15–18] and electrorotation.[19–22] For an initial spherical drop of radius a subject to an electric field of magnitude E_0, the characteristic electric stress is εE_0^2, where ε is the permittivity of the suspending fluid. The ratio of the stresses due to the electric field and surface tension defines the electric capillary number $Ca = \varepsilon E_0^2 a/\gamma$, where γ is the interfacial tension. It is an important non-dimensional quantity that decides the shape of the drop in electrohydrodynamic flows. For $Ca \ll 1$, the drop shape will remain spherical. In this study, we assume $Ca \ll 1$. To justify this assumption, let us consider a water droplet of radius $10\,\mu$m suspended in air with $E_0 = 10^5\ \mathrm{V\ m}^{-1}$, $\varepsilon = \varepsilon_0 = 8.85 \times 10^{-12}\ \mathrm{F\ m}^{-1}$, and $\gamma = 72 \times 10^{-3}\ \mathrm{N\ m}^{-1}$. We find that $Ca \approx 0.0012$ is sufficiently small for neglecting drop deformation. Drop exhibits

interesting deformation dynamics for $Ca \gg 1$, and to know more about this topic, we would refer the reader to the recent review paper by Vlahovska.[16] A background flow[23–26] or drop inertia[27] can also deform the drop in the absence of an electric field. We assume that these driving forces for the drop deformation are not present in this study. The current study analyzes the relative motion of two spherical particles due to an external electric field. For two drops in Stokes flow, deformability becomes significant when the lubrication pressure between the two drops becomes comparable to the Laplace pressure. Gopinath and Koch[28] showed that the gap thickness (in μm) for which deformation becomes important is approximately $6.74 \times 10^{-5} a^{*2}$, where a^* is the average radius (in μm) of the interacting spheres. We ignore the surface deformations induced by the lubrication pressure, a reasonable assumption for smaller droplets where additional physics, such as van der Waals attraction and non-continuum effects, will occur before deformation.[29]

Even though the classical problem of a single drop in a uniform electric field has received extensive treatment, studying the dynamics of interacting drops due to induced dipoles and electrohydrodynamic flows is a domain of active interest. Recent studies have investigated the electrohydrodynamic interactions between two drops experimentally and numerically when the drop pair is aligned with the external field.[30–32] For small drop deformations, Vlahovska and coauthors[33–36] analyzed the three-dimensional electrohydrodynamic interactions of a drop pair using the boundary integral method and an asymptotic theory for large separations. They elucidated complex drop trajectories by linking them with non-reciprocal interactions caused by the electrohydrodynamic flows. Kach *et al.*[37] investigated a similar problem for pairwise interactions between three or more drops. In this study, we neglect the electrohydrodynamic interactions between drop pairs and consider that drops interact via electric-field-induced forces that arise due to electric polarization. Previous studies analyzed the effects of electric-field-induced forces on relative trajectories for two uncharged conducting rigid spherical particles in a simple shear flow[38] and two uncharged conducting non-deformable viscous drops settling under gravity.[39] However, they have not considered appropriate lubrication forms for the electric-field-induced forces. Here, we derive the asymptotic expressions for the field-induced forces to analyze the near-field interactions between two uncharged conducting spheres of arbitrary size ratios. We show that the divergent nature of the electric-field-induced force in the lubrication region can lead to surface-to-surface contact between the spheres in a finite time, even without any other nonhydrodynamic attractive forces. Thus, our study has important implications in the context of electrocoagulation or electrocoalescence.

An external electric field induces electrical charges of the opposite sign on the nearest surfaces of the two uncharged conducting spheres. The electrostatic attraction between induced charges drives the relative motion between the particles. As the two spheres come closer to each other, the strength of the electric field in the region of nearby points of the two spheres becomes much higher than the imposed field.[40] Most importantly, this enhancement increases without limit as the separation tends to zero.[41] However, the electric-field-induced forces become negligible for large interparticle separations. Thus, the electric-field-induced forces alone cannot bring two widely separated particles into contact unless the drop pairs come close enough due to an imposed flow or gravity. Gravitational and Brownian motion-induced forces, among others, can drive the relative motion between a pair of widely separated drops dispersed in a quiescent fluid. We assume that the effect of gravity is negligible due to a small particle size, but at the same time, the particles are large enough so that the Brownian diffusion is negligible. Here, we analyze the role of electric-field-induced forces on pair trajectories of two uncharged conducting drops in close approach.

The effects of an external electric field on the electrostatic interactions between two uncharged or charged conducting spheres have been studied extensively. Davis[40] solved the Laplace equation for the electric potential field using the separation of variables in bispherical coordinates to determine the variation of the disturbed electric field in the regions excluding the two spheres and the induced surface charges on the spheres. Love[42] derived the analytical expressions for the dipole moment of two equal-sized uncharged dielectric spheres in an external electric field. O'Meara, Jr. and Saville[43] solved the boundary value problem for the electrostatic interactions between two touching conducting spheres in an external electric field and derived the capacitance, induced charge, and force on each sphere. Stoy[44,45] solved the potential field (inside and outside of the two spheres) for different sizes and different permittivities in an imposed electric field directed along and normal to the line joining the centers. The solution procedure mentioned in these studies yields series expressions for the electrostatic force between two uncharged spherical conductors. When the gap thickness between the two spheres tends to zero, the convergence of these series becomes computationally expensive as these series require many terms. One needs the equivalent analytical expressions of these series in close separations to overcome this convergence issue. Friesen and Levine[46] calculated the electric-field-induced forces of a system of two uncharged spheres by finding the electrostatic energy of the system due to an imposed uniform electric field. They noted that only dipole moment components along and normal to the line joining centers contribute to the system energy. Later, Lekner[47] extended the formulation of Friesen and Levine[46] to a system of uncharged spherical conductors by generalizing Landau and Lifshitz's[48] theorem for a single uncharged spherical conductor. Lekner[47] expressed the system energy in terms of the polarizability tensor. For calculating the electrostatic energy and forces in the case of a two-sphere system, only longitudinal and transverse components of the polarizability tensor are sufficient.[47] To calculate the electric-field-induced forces at a small interparticle distance, we utilize the work of Lekner,[49] who derived the exact analytical expressions for the longitudinal and transverse polarizabilities in close separations of the two spheres of arbitrary size ratio. The forces acting along the line joining the centers of the two spheres are equal and opposite and related to the derivatives of the polarizabilities with respect to the separation. The force normal to the line of centers produces torque on the two-sphere system, which is proportional to the difference between the longitudinal and transverse polarizabilities. This torque always acts to align the line of centers with the direction of the external electric field.

For small to moderate separations, two spheres disturb the velocity fields around each other. These disturbances increase the hydrodynamic resistance on each sphere. Thus, apart from electrostatic interactions, spheres interact with each other through hydrodynamic interactions (HI). The effects of hydrodynamics interactions on the relative motion between a pair of spheres in Stokes flow conditions are well studied.[50] The hydrodynamic resistance significantly reduces the relative velocity in close separations, and it depends on the two-sphere

relative geometry (i.e., center-to-center distance and size ratio). The separation between two spheres is $r - a_1 - a_2$, where r is the center-to-center distance, and a_1 and a_2 are the radius of spheres 1 and 2, respectively. We denote ξ as the dimensionless [non-dimensionalized by $a^* = (a_1 + a_2)/2$, the average radius of the two spheres] separation. Thus, $\xi = (r/a^*) - 2$, where r/a^* is the non-dimensional center-to-center distance. The hydrodynamic resistance in the lubrication region is $O(1/f(\xi))$. The function $f(\xi) = \xi$ for two rigid spheres with continuum hydrodynamic interactions[51] and $f(\xi) = \sqrt{\xi}$ for two spherical viscous drops interacting via continuum hydrodynamics.[52] For spheres interacting in a gaseous medium, the continuum lubrication approximation is no longer valid, and one needs to consider non-continuum lubrication resistance with $f(\xi) = \ln(\ln(Kn/\xi))/Kn$.[29,53] Here, Kn, the Knudsen number that captures the significance of non-continuum interactions, is defined as the ratio of the mean free path of the medium to the mean radius of the interacting spheres. In the present problem, we determine the relative trajectories of two spheres in a vertical electric field, while the spheres interact through continuum hydrodynamics.

This study analyzes the near-field interaction of two arbitrary-sized uncharged spherical conductors subject to an external electric field. We also take into account the hydrodynamic interactions between the conductors. In Sec. II, we derive the pair trajectory equation of uncharged conducting spheres in an electric field. We discuss the relation between electric-field-induced forces and polarizabilities for small and large separations in Sec. III and show typical pair trajectories in Sec. IV A. In Secs. IV B and IV C, we analyze the trajectory of two uncharged spheres when the electric field acts along and normal to the line of centers. Finally, in Sec. V, we summarize our results and discuss their implications.

II. PAIR TRAJECTORY EQUATION

We consider a dilute dispersion of uncharged conducting spheres subject to a vertically downward electric field. We assume that the fluid surrounding the particles is quiescent, i.e., there is no background flow. The terminal speed of a particle settling under gravity in a still fluid is proportional to the square of the particle radius, and particle inertia based on the settling timescale varies with the cube of the particle radius. In the current analysis, we assume that particles are small enough for gravitational settling and particle inertia to be negligible but large enough to ignore the Brownian diffusion. Effectively, we are considering a scenario where an external electric field drives the motion of the particles (i.e., the dispersed phase). For dilute dispersions, the interactions between three or more particles are unlike, and thus, we carry out the analysis for binary interactions, as shown in Fig. 1. Finally, we assume that the disturbance flow field generated by the movements of the particles is sufficiently slow, and thus, Stokes equations can appropriately describe the flow field.

Let $\boldsymbol{F}_1$ and $\boldsymbol{F}_2$ be the external forces acting on spheres 1 and 2, respectively, including hydrodynamic interactions, the instantaneous velocities of the two spheres can be written as[54]

$$\boldsymbol{U}_1 = \boldsymbol{M}_{11} \cdot \boldsymbol{F_1} + \boldsymbol{M}_{12} \cdot \boldsymbol{F_2}, \tag{1}$$

$$\boldsymbol{U}_2 = \boldsymbol{M}_{21} \cdot \boldsymbol{F_1} + \boldsymbol{M}_{22} \cdot \boldsymbol{F_2}, \tag{2}$$

where $\boldsymbol{U}_1$ and $\boldsymbol{U}_2$ are the velocities of spheres 1 and 2, respectively, $\boldsymbol{M}_{\alpha\beta}$ $(\alpha, \beta = 1, 2)$ are the hydrodynamic mobility tensors. Since the two-sphere system is symmetric about the line joining the centers, we can write $\boldsymbol{M}_{\alpha\beta}$ as

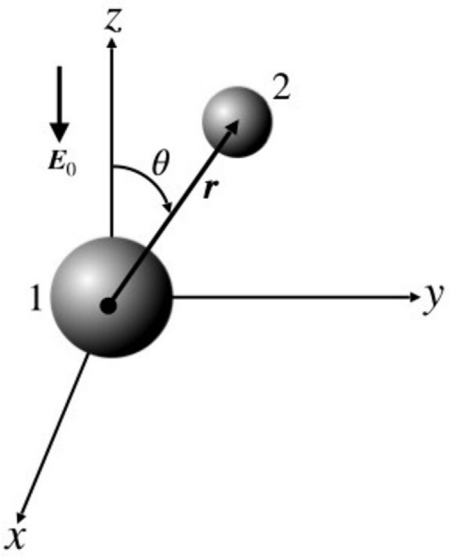

FIG. 1. Geometric representation of two spheres' interactions in spherical coordinates. Here, "1" represents the sphere with radius a_1, and "2" represents the sphere with radius a_2.

$$\boldsymbol{M}_{\alpha\beta} = \frac{1}{3\pi\mu_f(a_\alpha + a_\beta)}\left[A_{\alpha\beta}\frac{\boldsymbol{rr}}{r^2} + B_{\alpha\beta}\left(\boldsymbol{I} - \frac{\boldsymbol{rr}}{r^2}\right)\right], \tag{3}$$

where $\boldsymbol{r}$ is the vector from the center of particle 1 to the center of particle 2, $r = |\boldsymbol{r}|$, $\boldsymbol{I}$ is a rank two identity tensor, μ_f is the dynamic viscosity of the surrounding fluid, and $A_{\alpha\beta}$ and $B_{\alpha\beta}$ are the mobility functions that depend on the geometry of the two-sphere configuration. The electric-field-induced forces on the two spheres are equal and opposite, i.e., $\boldsymbol{F}_1 = -\boldsymbol{F}_2 = \boldsymbol{F}$. Thus, the relative velocity $\boldsymbol{V}_{12} = \boldsymbol{U}_2 - \boldsymbol{U}_1$ between the particle pair can be written as

$$\boldsymbol{V}_{12} = (\boldsymbol{M}_{11} + \boldsymbol{M}_{22} - \boldsymbol{M}_{12} - \boldsymbol{M}_{21}) \cdot \boldsymbol{F}. \tag{4}$$

After substituting the expression for the mobility tensors in Eq. (4), we have

$$\boldsymbol{V}_{12} = \frac{1}{6\pi\mu_f}\left(\frac{1}{a_1} + \frac{1}{a_2}\right)\left[G\frac{\boldsymbol{rr}}{r^2} + H\left(\boldsymbol{I} - \frac{\boldsymbol{rr}}{r^2}\right)\right] \cdot \boldsymbol{F}, \tag{5}$$

where G and H can be expressed in terms of $A_{\alpha\beta}$ and $B_{\alpha\beta}$. Here, $\boldsymbol{F}$ is a function of both r and θ, and thus, we need to consider both axisymmetric and asymmetric relative motions. Furthermore, G and H are axisymmetric mobility (responsible for the relative motion along the line of centers) and asymmetric mobility (responsible for the relative motion normal to the line of centers) functions, respectively. These mobility functions depend on the size ratio $\kappa = a_2/a_1$ and dimensionless center-to-center distance r/a^*. These scalar mobility functions (G, H) do not depend on the surrounding fluid properties for suspensions of rigid spherical particles. For suspensions of viscous drops, G and H additionally depend on the drop-to-medium viscosity ratio. Different techniques for determining these mobility functions include

twin-multipole expansions[55] boundary-multipole collocation[50] and Stokes equation solution in bispherical coordinates.[56,57] This study uses twin-multipole expansions to obtain the asymmetric mobility H functions and solutions in bispherical coordinates to obtain the axisymmetric mobility G. These mobility functions for continuum hydrodynamic interactions have analytical expressions in far field and near field.[54,58] For $\xi \to 0$, expressions for G and H are given by

$$G \sim \frac{(1+\kappa)^2}{2\kappa}\xi, \tag{6}$$

$$H \sim H(\xi = 0) + \frac{\text{const.}}{\ln \xi^{-1}}. \tag{7}$$

Similarly, the asymptotic expressions for G and H for large separation are

$$G = 1 - \frac{6\kappa}{(1+\kappa)^2}\frac{1}{r} + O(r^{-3}), \tag{8}$$

$$H = 1 - \frac{3\kappa}{(1+\kappa)^2}\frac{1}{r} + O(r^{-3}). \tag{9}$$

Here, r is the non-dimensional (scaled by a^*) center-to-center distance between the spheres.

To determine the relative trajectories, we choose a spherical coordinate system (r, θ, ϕ) with origin at the center of sphere 1 and then track the center of sphere 2. We use the mean radius of the two spheres as the characteristic length scale. Therefore, the non-dimensional radial separation between the centers of the two spheres can lie in the range of 2 to ∞. Now onward, we will denote r as the non-dimensional center-to-center distance. The size ratio κ, which can vary in the range $(0, 1]$, captures the geometry of the two-sphere system. One must note here that Maxwell[59] in his original work measured the relative sphere size by defining $\beta = a_2/(a_1 + a_2)$, which lies in the range of 0 to 1. As the problem is axisymmetric, with the $z-$axis being the axis of symmetry, the azimuthal component of the relative velocity must be zero. After simplifying Eq. (5), the relative velocity in the radial and polar directions can be written as

$$V_r = \frac{dr}{dt} = \frac{1}{6\pi\mu_f}\left(\frac{1}{a_1} + \frac{1}{a_2}\right)GF_r, \tag{10}$$

$$V_\theta = r\frac{d\theta}{dt} = \frac{1}{6\pi\mu_f}\left(\frac{1}{a_1} + \frac{1}{a_2}\right)HF_\theta, \tag{11}$$

where F_r and F_θ are the electric-field-induced forces along the r and θ directions, respectively. From Eqs. (10) and (11), we have the following equation for the relative trajectory:

$$\frac{dr}{d\theta} = \frac{rV_r}{V_\theta} = r\frac{GF_r}{HF_\theta}. \tag{12}$$

The above equation for the relative trajectory represents a two-dimensional dynamical system. In Sec. IV, we will show that the two fixed points of the system lie on the contact sphere ($r = 2$) with $\theta = \pi/2$ and $3\pi/2$.

III. ELECTRIC-FIELD-INDUCED FORCES

In this section, we will discuss the electric-field-induced forces on two uncharged conducting spherical particles. Davis[40] derived the electrostatic forces between two charged conducting spheres in an impressed electric field by solving the Laplace equation for the electrical potential in a bispherical coordinate system. The force expressions given in Davis[40] involve ten force coefficients, namely, $F_1, F_2, \ldots, F_{10}$. For interactions between charged spheres in the absence of an electric field, only F_5, F_6, and F_7 are required, and in that case, the electrostatic attraction goes to infinity as the separation goes to zero.[60–62] In the present analysis, the coefficients F_1, F_2, and F_8 can capture the electric-field-induced forces between two uncharged spherical conductors. By dropping the terms involving the surface charges in the force expressions given by Davis,[40] we get the following expressions for the electric-field-induced forces along and normal to the line-of-centers of the two spheres:

$$F_r = -4\pi\varepsilon a_2^2 E_0^2(F_1\cos^2\theta + F_2\sin^2\theta), \tag{13}$$

$$F_\theta = 4\pi\varepsilon a_2^2 E_0^2(F_8\sin 2\theta), \tag{14}$$

where E_0 is the magnitude of the electric field, ε is the permittivity of the medium, and F_1, F_2, and F_8 are the force coefficients that depend on the non-dimensional separation and size ratio of the interacting pairs. These force coefficients are non-trivial series expressions that need to be solved numerically. The numerical convergences of these coefficients are extremely slow in close separations, and these series require many terms to achieve converged results.

To avoid the convergence issues, we use the work of Lekner,[49] who derived the analytical expressions for these forces in the near field for equal-sized spherical conductors. The external electric field induces charges on the sphere surface; hence, a net dipole moment develops in each conductor. These dipole moments can be written in terms of the polarizability tensor and the electric field vector. The polarizability tensor for a two-sphere system is isotropic and, thus, involves only three independent non-zero elements. The axisymmetric nature of the two-sphere geometry further reduces the number of variables to two. Therefore, only two quantities can appropriately describe the tensor: longitudinal polarizability (α_l) and transverse polarizability (α_t). The forces on the two-sphere system acting along and normal to the line joining the two centers depend on these two polarizabilities, the magnitude of the external electric field, and the angle the electric field vector makes with the line joining the centers. The force on sphere 2 in terms of the above quantities is given by[47]

$$F_r = \frac{4\pi\varepsilon E_0^2}{2}\left[\frac{\partial\alpha_t}{\partial r}\sin^2\theta + \frac{\partial\alpha_l}{\partial r}\cos^2\theta\right], \tag{15}$$

$$F_\theta = -\frac{4\pi\varepsilon E_0^2(\alpha_l - \alpha_t)\sin\theta\cos\theta}{r}. \tag{16}$$

Comparing (13) with (15) and (14) with (16), we get

$$F_1 = -\frac{1}{2a_2^2}\frac{\partial\alpha_l}{\partial r}, \tag{17}$$

$$F_2 = -\frac{1}{2a_2^2}\frac{\partial\alpha_t}{\partial r}, \tag{18}$$

$$F_8 = -\frac{1}{2a_2^2}\frac{(\alpha_l - \alpha_t)}{r}. \tag{19}$$

In Secs. III A and III B, we will present the near-field and far-field analytical expressions of these force coefficients for the arbitrary size ratio,

extending the results of Lekner[47] that were derived for two equal-sized spheres.

A. Force coefficients for small separations

The polarizabilities of a system of two uncharged conducting spheres depend on the radii of the spheres and the center-to-center distance between them. Exact series expressions for the longitudinal and transverse polarizabilities for the arbitrary size ratio are available in the literature.[47,49] The convergence of the series becomes a problem for small interparticle separations, particularly when the separation is less compared to the radii of the spheres. Lekner[49] obtained the close-form expressions for these polarizabilities by converting the series sums into integrals. The expressions for α_l and α_t are given by

$$\alpha_l = a_2^3(1-\lambda)^3\left[4\zeta(3) - \psi''(\lambda) - \psi''(1-\lambda) + \frac{M(\xi,\lambda)}{N(\xi,\lambda)}\right], \tag{20}$$

$$\alpha_t = a_2^3(1-\lambda)^3\left[Z_\lambda + \frac{\xi}{2\lambda(1-\lambda)}T_\lambda\right], \tag{21}$$

where $\lambda = \kappa/(1+\kappa)$, $\zeta(3) = 1.202\,056\,9\ldots$, and ψ is a digamma function. The expressions for the other variables involved in Eqs. (20) and (21) are given by

$$M(\xi,\lambda) = \frac{1}{2}\left[\psi'(\lambda) - \psi'(1-\lambda)\right]^2 \ln\left(\frac{4\lambda(1-\lambda)}{\xi}\right) - \frac{\pi^4}{36}F_\lambda - \frac{\pi^2}{3}G_\lambda - H_\lambda, \tag{22}$$

$$N(\xi,\lambda) = b + c\ln\xi, \tag{23}$$

$$Z_\lambda = -2\zeta(3) - \frac{1}{2}\psi''(\lambda) - \frac{1}{2}\psi''(1-\lambda), \tag{24}$$

$$T_\lambda = F_\lambda + (1 - 3\lambda + 3\lambda^2)Z_\lambda + Q_\lambda, \tag{25}$$

$$F_\lambda = \psi(\lambda) + \psi(1-\lambda) + 2\gamma, \tag{26}$$

$$G_\lambda = \psi(\lambda)\psi'(1-\lambda) + \psi'(\lambda)\psi(1-\lambda) + \gamma\left[\psi'(\lambda) + \psi'(1-\lambda)\right], \tag{27}$$

$$H_\lambda = \psi(\lambda)\psi'(1-\lambda)^2 + 2\gamma\psi'(\lambda)\psi'(1-\lambda) + \psi'(\lambda)^2\psi(1-\lambda), \tag{28}$$

$$Q_\lambda = \frac{1}{6}\lambda(1-\lambda)(2\lambda-1)\left[\psi'''(\lambda) - \psi'''(1-\lambda)\right], \tag{29}$$

$$b = \frac{1}{2}F_\lambda \ln\left(4\lambda(1-\lambda)\right) + \gamma^2 - \psi(\lambda)\psi(1-\lambda), \tag{30}$$

$$c = -\frac{F_\lambda}{2}. \tag{31}$$

Here, $\gamma = 0.577\,215\,664\,9\ldots$ is the Euler constant. Expressions (20)–(31) are valid at close approach only, at best up to a separation equal to the smaller of the two radii. Mathematically, these equations are useful up to $\xi/2\lambda(1-\lambda) \approx 0.1$.[49] Now, we will take the partial derivatives of α_l and α_t with respect to r. Note here that the derivative with respect to r is equivalent to the derivative with respect to ξ because $r = \xi + 2$. Thus, we have

$$\frac{\partial\alpha_l}{\partial\xi} = -\frac{(1-\lambda)a_2^2 C_\lambda}{\xi(b + c\ln\xi)^2}, \tag{32}$$

$$\frac{\partial\alpha_t}{\partial\xi} = a_2^2(1-\lambda)^2 T_\lambda, \tag{33}$$

where

$$C_\lambda = \lambda(1-\lambda)^2\left[\left[\psi'(\lambda) - \psi'(1-\lambda)\right]^2\left(\gamma^2 - \psi(\lambda)\psi(1-\lambda)\right) + F_\lambda\left(\frac{\pi^4}{36}F_\lambda + \frac{\pi^2}{3}G_\lambda + H_\lambda\right)\right]. \tag{34}$$

Finally, the force coefficients can be expressed as

$$F_1 \sim \frac{(1-\lambda)C_\lambda}{2\xi(b + c\ln\xi)^2}, \tag{35}$$

$$F_2 \sim -\frac{(1-\lambda)^2}{2}T_\lambda, \tag{36}$$

$$F_8 \sim -\frac{\lambda(1-\lambda)^3}{\xi+2}\left[\frac{M(\xi,\lambda)}{N(\xi,\lambda)} - \frac{\xi}{2\lambda(1-\lambda)}T_\lambda + 8\zeta(3) + z_\lambda\right]. \tag{37}$$

We find (also reported in Table I of Davis[40]) that the numerical values of F_1 are positive and those of F_2 and F_8 are negative. We also find that the force along the line of centers is attractive (i.e., $F_r < 0$) in close approach except for the situation when the angle between the electric field and the line joining the centers is close to $\pi/2$. On the other hand, the tangential force F_θ is always repulsive, and thus, the torque acting on the system always tries to align the line of centers with the electric field. From the near-field analytical forms of F_1 and F_2, we can conclude that the attractive force (except for $\theta \sim \pi/2$) $F_r = O(\xi^{-1}[\ln\xi]^{-2})$ for $\xi \to 0$, which means that the attractive force increases without bound as the spheres approach each other. The crossover angle between attraction and repulsion between the spheres depends on ξ and λ. Mathematically, the crossover angle is the value of θ when $F_r = 0$. For small separations, the crossover angle is given by

$$\tan^2\theta = \frac{C_\lambda}{T_\lambda(1-\lambda)\xi(b + c\ln\xi)^2}. \tag{38}$$

Figure 2 shows the variation of F_1, F_2, and F_8 with ξ when $\kappa = 0.5$. The dashed lines in the figure indicate the behavior of the force

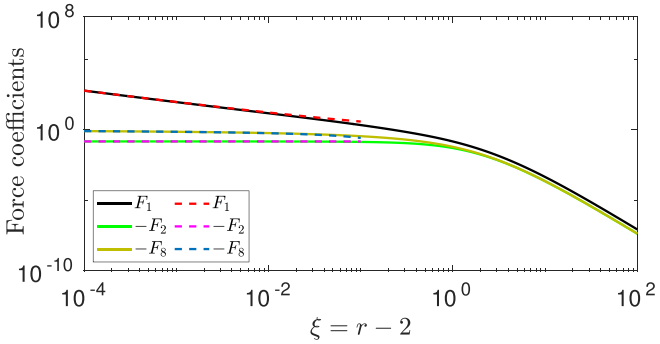

FIG. 2. The magnitudes of the force coefficients F_1, F_2, and F_8 are plotted as a function of separation $\xi = r - 2$ when the size ratio $\kappa = 0.5$. The continuous lines indicate numerically obtained solutions for F_1, F_2, and F_8 (see Davis[40] for details), while the corresponding dashed lines are analytical solutions in the lubrication regime.

coefficients in small separations. In Fig. 3, we show the normalized F_r and F_θ (normalized by $4\pi\varepsilon a_2^2 E_0^2$) in $\kappa-\theta$ parameter space when the spheres are almost in contact ($\xi = 10^{-6}$). It is evident from this plot that the magnitudes of forces both along and normal to the line joining the centers are maximum for spheres with equal sizes. The physical reason behind this is that equal-sized spheres experience the largest effects of mutual polarization. Figure 3(a) indicates that the strength of F_r is maximum when the line joining the sphere centers aligns with the electric field (i.e., $\theta = 0$), and it reduces monotonically as θ approaches $\pi/2$. Most importantly, for θ values around $\pi/2$, F_r is repulsive (i.e., $F_r > 0$). As expected, F_θ is zero when $\theta = 0, \pi/2$ and maximum when $\theta = \pi/4$ [see Fig. 3(b)]. This behavior of both F_r and F_θ in the $\kappa-\theta$ plane is qualitatively similar for all separations.

B. Force coefficients for large separations

The longitudinal and transverse polarizabilities for large interparticle separations are given by (see Ref. 47):

$$\alpha_l = a_1^3 + a_2^3 + \frac{4a_1^3a_2^3}{r^3} + \frac{4a_1^3a_2^3(a_1^3+a_2^3)}{r^6} + O(r^{-8}), \tag{39}$$

$$\alpha_t = a_1^3 + a_2^3 - \frac{2a_1^3a_2^3}{r^3} + \frac{a_1^3a_2^3(a_1^3+a_2^3)}{r^6} + O(r^{-8}). \tag{40}$$

Using Eqs. (39) and (40), we get the following far-field expressions for the force coefficients:

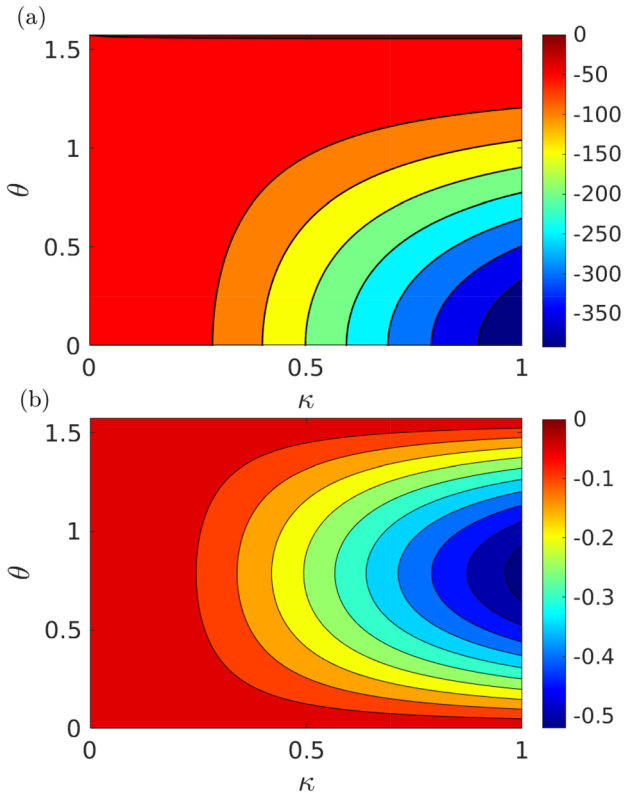

FIG. 3. Contour plots of (a) normalized F_r and (b) normalized F_θ in the $\kappa-\theta$ parameter space when the separation between the spheres $\xi = 10^{-4}$.

$$F_1 = \frac{96\lambda(1-\lambda)^3}{r^4} + O(r^{-7}), \tag{41}$$

$$F_2 = -\frac{48\lambda(1-\lambda)^3}{r^4} + O(r^{-7}), \tag{42}$$

$$F_8 = -\frac{48\lambda(1-\lambda)^3}{r^4} + O(r^{-7}). \tag{43}$$

The above three forms of the force coefficients suggest that both F_r and F_θ decay as $O(r^{-4})$ for $r \to \infty$. The crossover angle θ between attraction and repulsion between the spheres for large separations is given by

$$\theta = \cos^{-1}\left(\sqrt{\frac{-F_2}{F_1 - F_2}}\right) = \cos^{-1}\left(\frac{1}{\sqrt{3}}\right) \approx 55^\circ. \tag{44}$$

IV. RESULTS AND DISCUSSION

A. Typical pair trajectories

Here, we discuss the relative trajectories of two uncharged spherical conductors in the presence of hydrodynamic interactions and electric-field-induced forces. Contact forces between the spheres arise after they make surface-to-surface contact (i.e., when $\xi = 0$) (see Lekner[63] for the derivations of contact forces). However, we are interested in the pre-collision dynamics, and thus, we focus our attention on the relative trajectories in close approach (i.e., $\xi \to 0$). Therefore, we will not consider contact forces in our analysis. As the relative motion of the two spheres does not depend on the azimuthal coordinate ϕ [see Eq. (12)], without any loss of generality, we can carry out the analysis in a plane that is orthogonal to the x–y plane and contains z-axis. Therefore, we present the phase portrait in a generic $r\sin\theta$-$r\cos\theta$ plane. The close-form analytical solution of Eq. (12) is not possible except for the cases where the initial angle between the external electric field and the line of centers is either 0 or $\pi/2$. We integrate Eq. (12) numerically using a fourth-order Runge–Kutta method for various initial θ on the surface of the excluded volume sphere of non-dimensional radius 2. Figure 4 shows the typical pair trajectories for a pair of equal-sized spheres interacting through continuum hydrodynamics and electric-field-induced forces. Except for initial $\theta = 0, \pi/2, \pi$, and $3\pi/2$, the sphere centers follow the trajectories either in the first and third or second and fourth quadrants. The sphere centers move along the axis of the external field when the initial $\theta = 0, \pi$ and perpendicular to the field direction when $\theta = \pi/2, 3\pi/2$. In Secs. IV B and IV C, we will present the analytical solutions of the trajectory equation for these special cases. We find that all the trajectories in the positive side of $r\sin\theta$ start from $r = 2$, $\theta \approx \pi/2$ and hit the excluded surface at different θ locations. The trajectories in the negative side of $r\sin\theta$ originate from $r = 2$, $\theta \approx 3\pi/2$. It is important to note here that the trajectories on either side of $r\sin\theta$ are topologically similar. The sphere centers move with different velocities along their trajectories. For a given r, θ, these velocities can be calculated using Eqs. (10) and (11).

The dynamics of pair trajectories in the close approach of interacting spheres have significant implications in the context of electrocoagulation/electrocoalescence of uncharged particles in a suspension subject to an external electric field. As expected, the trajectory analysis demonstrates that an external field always acts to orient a pair of adjacent spherical particles along the direction of the impressed electric

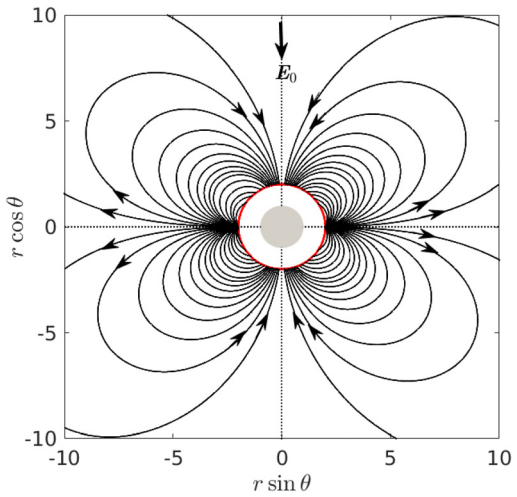

FIG. 4. Typical pair trajectories of two equal-sized uncharged conducting spheres subject to a vertical electric field. The sphere at the center is the reference sphere, and the red colored circle represents the excluded volume sphere in the plane. The arrows indicate the directions of the trajectories. We have considered the continuum hydrodynamic interactions between the spheres as they move around. Relative trajectories without hydrodynamic interactions are qualitatively similar to those with interactions.

field. Most importantly, two spherical conductors can come into contact in a finite time and form a doublet. The mathematical justification for finite time contact is that the force coefficient F_1 has a $O(\xi^{-1}[\ln \xi]^{-2})$ singularity near contact, which means that the attraction force between the spheres increases without bound as they come close. Thus, the external field causes flocculation of the suspension. The behavior of the interaction forces near contact dictates the collision dynamics of particles suspended in a liquid or gaseous medium. The electric-field-induced forces always promote the collision process and thus significantly enhance the flow-induced or gravity-induced collision rates.

B. Trajectory analysis for $\theta = 0, \pi$

In this subsection, we attempt to solve the trajectory equation for a specific case where the line of centers of the two spheres initially aligns with the external electric field. Substituting the expressions for F_r and F_θ from Eqs. (13) and (14) in the relative velocity Eqs. (10) and (11) and setting $\theta = 0$ or π, we have the following dimensionless trajectory equation:

$$\frac{dr}{dt} = -\frac{4\lambda}{3(1-\lambda)} G F_1, \tag{45}$$

where t is the dimensionless time scaled with $\mu_f/\varepsilon E_0^2$. The spheres have no relative motion in the tangential direction because the two-sphere system does not experience any torque when $\theta = 0, \pi$. Equation (45) suggests that the spheres will approach each other because of the attractive forces induced by the electric field. As we have stated earlier, the mathematical form of the relative velocity near contact decides whether the particle surfaces will touch each other in a finite time. Thus, we focus on the pair trajectories for small surface-to-surface distances. Without hydrodynamic interactions (i.e., $G = 1$), the dimensionless trajectory equation in close approach becomes

$$\frac{d\xi}{dt} \sim -\frac{a}{\xi(b + c\ln\xi)^2}, \tag{46}$$

where $\xi = r - 2$ and $a = 2\lambda C_\lambda/3$. We obtained (46) after substituting the near-field asymptotic form of F_1 in (45). Using the initial condition $\xi = \xi_0$ at $t = 0$, we get the following expression for t by analytically solving (46)

$$t = t_c - \frac{\left((b + c\ln\xi - c/2)^2 + (c/2)^2\right)\xi^2}{2a}, \tag{47}$$

where $t_c = \left((b + c\ln\xi_0 - (c/2))^2 + (c/2)^2\right)\xi_0^2/2a$ is the time taken by two spheres initially separated by a small distance ξ_0 to come into contact. So, for a given ξ_0, we can calculate t_c numerically. Though the analytical integration of Eq. (46) yields an implicit solution for ξ, we can express $\xi(t)$ explicitly in terms of t asymptotically. For $(t_c - t) \ll 1$, our asymptotic analysis gives

$$\xi \sim (t_c - t)^{1/2}\frac{1}{\sqrt{z_1}}\left(1 + \frac{c\ln z_1}{2\sqrt{2az_1}}\right), \tag{48}$$

where $z_1 = \left((b + (c/2)\ln(t_c - t) - (c/2))^2 + (c/2)^2\right)/2a$.

In the presence of hydrodynamic interactions, the mobility $G \sim O(\xi)$ as ξ approaches zero. After substituting the small separation asymptotic expressions for G and F_1 in (45), the near-field form of the trajectory equation with hydrodynamic interactions becomes

$$\frac{d\xi}{dt} \sim -\frac{m}{(b + c\ln\xi)^2}, \tag{49}$$

where $m = C_\lambda/3(1-\lambda)$. Using the same initial condition as before, we get the following solution for Eq. (49):

$$t = t_c - \frac{\left((b + c\ln\xi - c)^2 + c^2\right)\xi}{m}. \tag{50}$$

Here, $t_c = \left((b + c\ln\xi_0 - c)^2 + c^2\right)\xi_0/m$. Similar to the case without hydrodynamic interactions, we perform the asymptotic analysis in the $(t_c - t) \ll 1$ limit and obtain the following explicit expression for ξ in the presence of hydrodynamic interactions:

$$\xi \sim (t_c - t)\frac{1}{z_2}\left(1 + \frac{2c\ln z_2}{\sqrt{mz_2}}\right), \tag{51}$$

where $z_2 = \left((b + c\ln(t_c - t) - c)^2 + c^2\right)/m$.

Figure 5 shows how the separation between the spheres decreases with time, both in the absence and presence of hydrodynamic interactions. We present these results for two size ratios, 0.1 (significant difference in sizes) and 1.0 (equal in size). We choose $\xi_0 = 10^{-1}$ as the initial condition while integrating the trajectory equation. It is evident from the figure that the attraction force between the spheres increases rapidly as they approach each other, and it can lead to contact between the surfaces in a finite time t_c. For a given ξ_0, we determine t_c numerically. If we follow a curve in Fig. 5, we can see that the separation starts to decrease rapidly after a critical time. Numerically, we identify this time as the collision time t_c. This collision time is different for different initial separations ξ_0 and size ratio κ and for without and with hydrodynamic interactions. We use t_c as inputs in Eqs. (47) and (50) to plot

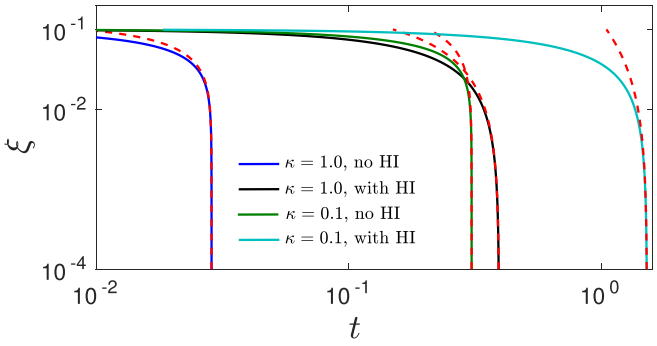

FIG. 5. Time evolution of interparticle separation in close approach of two spheres of size ratio $\kappa = 0.1, 1$ both without and with hydrodynamic interactions (HI) when the electric field aligns with the line joining the centers. The dashed lines corresponding to each continuous curves represent the analytical solutions.

ξ as a function of t, and we can see a good agreement between our numerical results (continuous lines in Fig. 5) and the analytical results (dashed lines in Fig. 5). Hydrodynamic interactions retard the dynamics. Thus, particles (of a given size ratio) interacting through continuum hydrodynamics take longer to come into contact compared to those without hydrodynamic interactions. We also observe that the rate of approach is faster for particle pairs with large size differences. To validate our asymptotic expressions without and with hydrodynamic interactions, we plot ξ as a function of $(t_c - t)$ in Fig. 6. Our asymptotic results (dotted lines in Fig. 6) are in good agreement with the numerical results (continuous lines in Fig. 6).

C. Trajectory analysis for $\theta = \pi/2, 3\pi/2$

Here, we analyze the time evolution of the pair trajectories when the line joining the centers of the two spheres is perpendicular to the direction of the external electric field. Like the previous case, the relative velocity between the spheres in the tangential direction is zero. In this case, the trajectory equation is given by

$$\frac{dr}{dt} = -\frac{4\lambda}{3(1-\lambda)} G F_2. \tag{52}$$

The electric-field-induced forces are repulsive in this configuration. As we have mentioned earlier, the numerical values of F_2 are negative, and thus, the radial relative velocity is positive (i.e., the spheres will move apart from each other). Substituting the expression of F_2 from Eq. (35) in Eq. (52), we get the trajectory equation in the lubrication regime as

$$\frac{d\xi}{dt} \sim \frac{2\lambda(1-\lambda)T_\lambda}{3} G. \tag{53}$$

With the same initial condition as the previous case, the near-field analytical solutions for ξ without and with hydrodynamic interactions are, respectively,

$$\xi = \xi_0 + \frac{2\lambda(1-\lambda)T_\lambda}{3} t, \tag{54}$$

and

$$\xi = \xi_0 \exp\left(\frac{T_\lambda}{3} t\right). \tag{55}$$

Similar to the near-field solution, the far-field solution for (52) is given by

$$r(t) \sim \left(r_0^5 + 320\lambda^2(1-\lambda)^2 t\right)^{1/5}, \tag{56}$$

where the initial separation r_0 is much larger than one.

Figure 7 shows the time evolution of ξ without and with hydrodynamic interactions for $\kappa = 0.1, 1.0$ when the electric field is perpendicular to the line joining the centers. We take the initial separation $\xi_0 = 10^{-6}$. In this case, the relative separation increases with time because of the repulsion force induced by the external electric field. Without hydrodynamic interactions, ξ increases linearly with t in the near field. In the near field, even though the separation increases exponentially with time in the presence of hydrodynamic interactions, the rate of this increment is low compared to that without hydrodynamic interactions cases. We report that the rate of increase in the relative separation is higher for particle pairs with higher κ. For a given size ratio, the curves without and with hydrodynamic interactions merge with each other at large time. Our far-field analytical solution shows

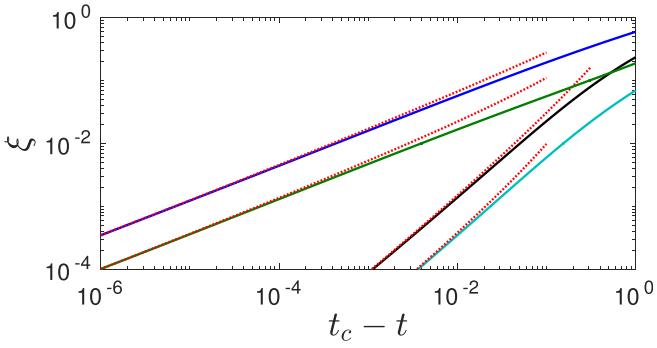

FIG. 6. Comparison of the numerical solution of the trajectory equation with the asymptotic expressions given in Eqs. (48) and (51). The legend for the continuous lines is the same as in Fig. 5. The dotted lines corresponding to each continuous curves represent asymptotic solutions.

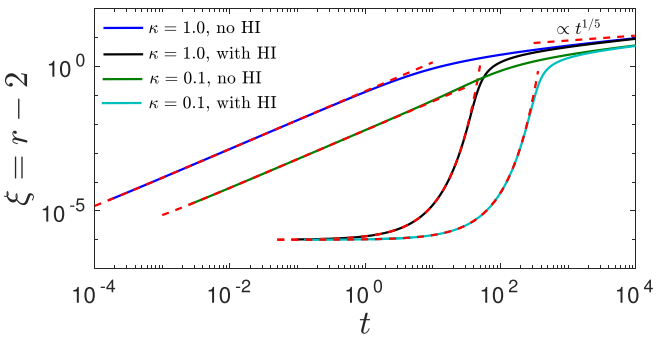

FIG. 7. Time evolution of interparticle separation of two spheres of size ratio $\kappa = 0.1, 1$ both without and with hydrodynamic interactions (HI) when the electric field is perpendicular to the line joining the centers. The dashed lines corresponding to each continuous curve represent the analytical solutions.

that $r(t)$ goes as $t^{1/5}$. The dashed lines in Fig. 7 are the analytical results, and these are in good agreement with the numerical results.

V. CONCLUSIONS

We have analyzed the effects of electrostatic forces on a pair of uncharged conducting spheres subject to an external electric field. We have also included the hydrodynamic interactions between the particle pair. Our present analysis borrows from classical and more recent studies on the electric-field-induced force and torque of a two-sphere system. It is well established that electric-field-induced forces are always attractive, except when the line of centers of the two spheres is perpendicular to the external electric field. The electric-field-induced torque always acts to align the line joining the sphere centers with the direction of the imposed field. We utilized the work of Davis[40] to calculate the field-induced forces on the system when the separation between the spheres is moderate to large. For calculating the forces in the near field, we derived the force coefficients for arbitrary size ratio using the work of Lekner,[49] who have provided the closed-form analytical expressions for the longitudinal and transverse polarizabilities of a system of two conducting spheres in close approach. We showed a typical map of pair trajectories, while spheres interact through electric-field-induced forces and continuum hydrodynamics. We have also presented how separations between the spheres evolve with time for two particular configurations. In one case, the pair were aligned with the electric field; in the other, they were in the perpendicular configuration.

The collision rate calculations of drops due to the combined effects of gravity,[29] turbulence,[64] particle inertia,[65] and electrostatic forces have important implications in several environmental and engineering scenarios. The evolution of drop size distribution in warm cumulus clouds significantly depends on the rate of collision between drops. The present study will help quantify the enhancement of drop collision rate due to electric-field-induced forces. The electrostatic attraction forces due to an electric field dominate the drop–drop coalescence process in strongly electrified clouds. The current study provides the near-field expressions for the electric-field-induced forces, which are essential to understand the collisional dynamics of drops in the presence of various driving forces like background flow and gravity. Recently, Melheim and Chiesa[66] and Lu *et al.*[67] used direct numerical simulations to study droplet size distributions and flow modulation in droplet-laden turbulent shear flows with an external electric field. Investigations on turbulent electrocoalescence would require incorporating better models of interparticle forces; the asymptotic forms of the electric-field-induced forces derived in the present study would be one such candidate. An extension of our study would be to analyze the effects of electric-field-induced forces on the collision rate of a pair of uncharged conducting drops settling in still air, accounting for non-continuum hydrodynamic interactions.

In the present study, we have assumed the drops as non-deformable conducting spheres. However, treating the drops as perfect conductors is an idealization, and most liquids are weakly conducting or leaky dielectrics. As was discussed earlier, several studies have investigated the deformation dynamics of a single drop in a strong electric field with finite charge relaxation effects taken into account.[15–18] Recently, researchers have developed theory and numerical schemes to capture the electrohydrodynamic interactions between two drops within the framework of the leaky dielectric model.[33–36] Future work could incorporate the derived asymptotic form of the electrostatic interactions to investigate electric-field-mediated interactions between drops in the weak deformation regime.

ACKNOWLEDGMENTS

The authors acknowledge the support from IIT Madras for its support of the "Laboratory for Atmospheric and Climate Sciences" research initiative under the Institute of Eminence framework. P.P. would like to acknowledge the financial support from the Prime Minister's Research Fellows (PMRF) scheme, Ministry of Education, Government of India (Project No. SB22230184AMPMRF008746).

AUTHOR DECLARATIONS

Conflict of Interest

The authors have no conflicts to disclose.

Author Contributions

Natarajan Thiruvenkadam: Data curation (equal); Formal analysis (equal); Visualization (equal); Writing – original draft (equal). **Pijush Patra:** Conceptualization (equal); Formal analysis (equal); Funding acquisition (equal); Visualization (equal); Writing – original draft (equal). **Vishwanath Kadaba Puttanna:** Supervision (equal); Writing – review & editing (equal). **Anubhab Roy:** Conceptualization (equal); Funding acquisition (equal); Investigation (equal); Visualization (equal); Writing – review & editing (equal).

DATA AVAILABILITY

The data that support the findings of this study are available within the article.

REFERENCES

[1]K. J. Ptasinski and P. J. A. M. Kerkhof, "Electric field driven separations: Phenomena and applications," Sep. Sci. Technol. **27**, 995–1021 (1992).
[2]M. G. Pollack, A. D. Shenderov, and R. B. Fair, "Electrowetting-based actuation of droplets for integrated microfluidics," Lab Chip **2**, 96–101 (2002).
[3]R. B. Karyappa, A. V. Naik, and R. M. Thaokar, "Electroemulsification in a uniform electric field," Langmuir **32**, 46–54 (2016).
[4]J. S. Eow and M. Ghadiri, "Electrostatic enhancement of coalescence of water droplets in oil: A review of the technology," Chem. Eng. J. **85**, 357–368 (2002).
[5]S. Less and R. Vilagines, "The electrocoalescers' technology: Advances, strengths and limitations for crude oil separation," J. Pet. Sci. Eng. **81**, 57–63 (2012).
[6]S. Mhatre and R. Thaokar, "Electrocoalescence in non-uniform electric fields: An experimental study," Chem. Eng. Process. **96**, 28–38 (2015).
[7]H. R. Pruppacher and J. D. Klett, *Microphysics of Clouds and Precipitation* (Kluwer Academic Publishers, 1997).
[8]J. R. Melcher and G. I. Taylor, "Electrohydrodynamics: A review of the role of interfacial shear stresses," Annu. Rev. Fluid Mech. **1**, 111–146 (1969).
[9]G. I. Taylor, "Studies in electrohydrodynamics. I. The circulation produced in a drop by an electric field," Proc. R. Soc. London, Ser. A **291**, 159–166 (1966).
[10]E. Lac and G. M. Homsy, "Axisymmetric deformation and stability of a viscous drop in a steady electric field," J. Fluid Mech. **590**, 239–264 (2007).
[11]R. B. Karyappa, S. D. Deshmukh, and R. M. Thaokar, "Breakup of a conducting drop in a uniform electric field," J. Fluid Mech. **754**, 550–589 (2014).
[12]G. I. Taylor, "Disintegration of water drops in an electric field," Proc. R. Soc. London, Ser. A **280**, 383–397 (1964).

[13]R. T. Collins, J. J. Jones, M. T. Harris, and O. A. Basaran, "Electrohydrodynamic tip streaming and emission of charged drops from liquid cones," Nat. Phys. **4**, 149–154 (2008).
[14]R. Sengupta, L. M. Walker, and A. S. Khair, "The role of surface charge convection in the electrohydrodynamics and breakup of prolate drops," J. Fluid Mech. **833**, 29–53 (2017).
[15]Q. Brosseau and P. M. Vlahovska, "Streaming from the equator of a drop in an external electric field," Phys. Rev. Lett. **119**, 034501 (2017).
[16]P. M. Vlahovska, "Electrohydrodynamics of drops and vesicles," Annu. Rev. Fluid Mech. **51**, 305–330 (2019).
[17]B. W. Wagoner, P. M. Vlahovska, M. T. Harris, and O. A. Basaran, "Electric-field-induced transitions from spherical to discocyte and lens-shaped drops," J. Fluid Mech. **904**, R4 (2020).
[18]B. W. Wagoner, P. M. Vlahovska, M. T. Harris, and O. A. Basaran, "Electrohydrodynamics of lenticular drops and equatorial streaming," J. Fluid Mech. **925**, A36 (2021).
[19]P. F. Salipante and P. M. Vlahovska, "Electrohydrodynamics of drops in strong uniform dc electric fields," Phys. Fluids **22**, 112110 (2010).
[20]H. He, P. F. Salipante, and P. M. Vlahovska, "Electrorotation of a viscous droplet in a uniform direct current electric field," Phys. Fluids **25**, 032106 (2013).
[21]D. Das and D. Saintillan, "Electrohydrodynamics of viscous drops in strong electric fields: Numerical simulations," J. Fluid Mech. **829**, 127–152 (2017).
[22]A. N. Tyatyushkin, "Unsteady electrorotation of a drop in a constant electric field," Phys. Fluids **29**, 097101 (2017).
[23]H. A. Stone, B. J. Bentley, and L. G. Leal, "An experimental study of transient effects in the breakup of viscous drops," J. Fluid Mech. **173**, 131–158 (1986).
[24]H. Yang, C. C. Park, Y. T. Hu, and L. G. Leal, "The coalescence of two equal-sized drops in a two-dimensional linear flow," Phys. Fluids **13**, 1087–1106 (2001).
[25]L. G. Leal, "Flow induced coalescence of drops in a viscous fluid," Phys. Fluids **16**, 1833–1851 (2004).
[26]M. Borrell, Y. Yoon, and L. G. Leal, "Experimental analysis of the coalescence process via head-on collisions in a time-dependent flow," Phys. Fluids **16**, 3945–3954 (2004).
[27]K. Sambath, V. Garg, S. S. Thete, H. J. Subramani, and O. A. Basaran, "Inertial impedance of coalescence during collision of liquid drops," J. Fluid Mech. **876**, 449–480 (2019).
[28]A. Gopinath and D. L. Koch, "Collision and rebound of small droplets in an incompressible continuum gas," J. Fluid Mech. **454**, 145–201 (2002).
[29]J. Dhanasekaran, A. Roy, and D. L. Koch, "Collision rate of bidisperse spheres settling in a compressional non-continuum gas flow," J. Fluid Mech. **910**, A10 (2021).
[30]S. Mhatre, S. Deshmukh, and R. M. Thaokar, "Electrocoalescence of a drop pair," Phys. Fluids **27**, 092106 (2015).
[31]V. Anand, S. Roy, V. M. Naik, V. A. Juvekar, and R. M. Thaokar, "Electrocoalescence of a pair of conducting drops in an insulating oil," J. Fluid Mech. **859**, 839–850 (2019).
[32]S. Roy, V. Anand, and R. M. Thaokar, "Breakup and non-coalescence mechanism of aqueous droplets suspended in castor oil under electric field," J. Fluid Mech. **878**, 820–833 (2019).
[33]C. Sorgentone, A.-K.Tornberg, and P. M. Vlahovska, "A 3D boundary integral method for the electrohydrodynamics of surfactant-covered drops," J. Comput. Phys. **389**, 111–127 (2019).
[34]C. Sorgentone, J. I. Kach, A. S. Khair, L. M. Walker, and P. M. Vlahovska, "Numerical and asymptotic analysis of the three-dimensional electrohydrodynamic interactions of drop pairs," J. Fluid Mech. **914**, A24 (2021).
[35]C. Sorgentone and P. M. Vlahovska, "Pairwise interactions of surfactant-covered drops in a uniform electric field," Phys. Rev. Fluids **6**, 053601 (2021).
[36]C. Sorgentone and P. M. Vlahovska, "Tandem droplet locomotion in a uniform electric field," J. Fluid Mech. **951**, R2 (2022).
[37]J. I. Kach, L. M. Walker, and A. S. Khair, "Prediction and measurement of leaky dielectric drop interactions," Phys. Rev. Fluids **7**, 013701 (2022).
[38]P. A. Arp and S. G. Mason, "Particle behaviour in shear and electric fields," Colloid Polym. Sci. **255**, 566–584 (1977).
[39]X. Zhang, O. A. Basaran, and R. M. Wham, "Theoretical prediction of electric field-enhanced coalescence of spherical drops," AIChE J. **41**, 1629–1639 (1995).
[40]M. H. Davis, "Two charged spherical conductors in a uniform electric field: Forces and field strength," Q. J. Mech. Appl. Math. **17**, 499–511 (1964).
[41]J. Lekner, "Near approach of two conducting spheres: Enhancement of external electric field," J. Electrost. **69**, 559–563 (2011).
[42]J. D. Love, "Dielectric sphere-sphere and sphere-plane problems in electrostatics," Q. J. Mech. Appl. Math. **28**, 449–471 (1975).
[43]D. O'Meara, Jr. and D. Saville, "The electrical forces on two touching spheres in a uniform field," Q. J. Mech. Appl. Math. **34**, 9–26 (1981).
[44]R. D. Stoy, "Solution procedure for the Laplace equation in bispherical coordinates for two spheres in a uniform external field: Parallel orientation," J. Appl. Phys. **65**, 2611–2615 (1989).
[45]R. D. Stoy, "Solution procedure for the Laplace equation in bispherical coordinates for two spheres in a uniform external field: Perpendicular orientation," J. Appl. Phys. **66**, 5093–5095 (1989).
[46]W. I. Friesen and S. Levine, "Electrostatic interaction between two water-in-oil emulsion droplets in an electric field," J. Colloid Interface Sci. **150**, 517–527 (1992).
[47]J. Lekner, "Forces and torque on a pair of uncharged conducting spheres in an external electric field," J. Appl. Phys. **114**, 224902 (2013).
[48]L. D. Landau and E. M. Lifshitz, *Electrodynamics of Continuous Media* (Pergamon Press, Oxford, 1960).
[49]J. Lekner, "Polarizability of two conducting spheres," J. Electrost. **69**, 435–441 (2011).
[50]S. Kim and S. J. Karrila, *Microhydrodynamics: Principles and Selected Applications* (Courier Corporation, 2013).
[51]G. K. Batchelor and J. T. Green, "The hydrodynamic interaction of two small freely-moving spheres in a linear flow field," J. Fluid Mech. **56**, 375–400 (1972).
[52]R. H. Davis, J. A. Schonberg, and J. M. Rallison, "The lubrication force between two viscous drops," Phys. Fluids A **1**, 77–81 (1989).
[53]R. R. Sundararajakumar and D. L. Koch, "Non-continuum lubrication flows between particles colliding in a gas," J. Fluid Mech. **313**, 283–308 (1996).
[54]G. K. Batchelor, "Sedimentation in a dilute polydisperse system of interacting spheres. Part 1. General theory," J. Fluid Mech. **119**, 379–408 (1982).
[55]D. J. Jeffrey and Y. Onishi, "Calculation of the resistance and mobility functions for two unequal rigid spheres in low-Reynolds-number flow," J. Fluid Mech. **139**, 261–290 (1984).
[56]C. J. Lin, K. J. Lee, and N. F. Sather, "Slow motion of two spheres in a shear field," J. Fluid Mech. **43**, 35–47 (1970).
[57]H. Wang, A. Z. Zinchenko, and R. H. Davis, "The collision rate of small drops in linear flow fields," J. Fluid Mech. **265**, 161–188 (1994).
[58]G. K. Batchelor, "Brownian diffusion of particles with hydrodynamic interaction," J. Fluid Mech. **74**, 1–29 (1976).
[59]J. C. Maxwell, *A Treatise on Electricity and Magnetism* (Clarendon Press, Oxford, 1873), Vol. 1.
[60]J. Lekner, "Electrostatics of two charged conducting spheres," Proc. R. Soc. London, Ser. A **468**, 2829–2848 (2012).
[61]A. S. Khair, "Electrostatic forces on two almost touching nonspherical charged conductors," J. Appl. Phys. **114**, 134906 (2013).
[62]P. Patra and A. Roy, "Brownian coagulation of like-charged aerosol particles," Phys. Rev. Fluids **7**, 064308 (2022).
[63]J. Lekner, *Electrostatics of Conducting Cylinders and Spheres* (AIP Publishing LLC, 2021).
[64]J. Dhanasekaran, A. Roy, and D. L. Koch, "Collision rate of bidisperse, hydrodynamically interacting spheres settling in a turbulent flow," J. Fluid Mech. **912**, A5 (2021).
[65]P. Patra, D. L. Koch, and A. Roy, "Collision efficiency of non-Brownian spheres in a simple shear flow—The role of non-continuum hydrodynamic interactions," J. Fluid Mech. **950**, A18 (2022).
[66]J. A. Melheim and M. Chiesa, "Simulation of turbulent electrocoalescence," Chem. Eng. Sci. **61**, 4540–4549 (2006).
[67]M. Lu, J. Lu, Y. Zhang, and G. Tryggvason, "Effect of electrostatic forces on the distribution of drops in turbulent channel flows," Phys. Fluids **31**, 105104 (2019).